Original Article

Linking the impact of seismicity on palaeogeographic evolution and sedimentary architecture: A case study from Middle Jurassic succession of Spiti Himalaya

Sabyasachi Mandal[1] , Abha Singh[1], Santanu Banerjee[2] , Premraj Uddandam[1] and Ranveer Singh Negi[1]

[1]Birbal Sahni Institute of Palaeosciences, Lucknow, India and [2]Department of Earth Sciences, Indian Institute of Technology Bombay, Powai, Mumbai, India

Abstract

The traces left by earthquakes in the unlithified sediments, recorded as soft-sediment deformation structures (SSDS), are well reconstructed as palaeo-seismic signals, while the origin of SSDS, seismic vs. Aseismic, is challenging. The present study discusses the origin of SSDS and its implications on palaeoceanography and sediment architecture. In the Middle Jurassic succession of Spiti Himalayan region in India, the topmost part of the Ferruginous Oolitic Formation (FOF) consists of four layers of SSDS and is underlain by the lower member of the Spiti Formation (SF). The sedimentary facies analysis documents the palaeogeographic shift from the middle shelf (carbonate-shale repository: FOF) to the outer shelf (black shale: lower member of SF). The SSDS layers, exhibiting load casts, ball and pillow structures, indicate gravitational instability, while syn-sedimentary faults and insitu breccia are the results of brittle deformation. The dominance of storms in depositional sites often argues for a possible triggering agent for SSDS. Therefore, it was necessary to distinguish between seismic vs. aseismic triggering agents. The lateral continuity, vertical repetition, confinement of SSDS at the top part of FOF and sharp change of facies assemblage indicate seismicity-induced syn-sediment deformation, i.e. seismite. The transition from middle shelf to outer shelf at the onset of seismite indicates that seismic impact possibly caused the rapid subsidence, resulting in the palaeogeographic shift. The rapid transgression is recorded as carbonate-shale repository to anoxic black shale. This study highlights the importance of sedimentological analysis to distinguish the seismite and its implications on palaeogeographic evolution and sedimentary architecture.

1. Introduction

Soft-sediment deformation structures (SSDS), typically form during or shortly after sedimentation, but prior to lithification, are observed in various sedimentary environments from mountain to deep sea (Sims, 1973, 1975; Quia *et al.* 1994; Sarkar *et al.* 1995; Owen, 1996; Owen *et al.* 2011; Owen and Moretti, 2011; He *et al.* 2014; Sarkar *et al.* 2014; Laborde-Casadaban *et al.* 2021). The primary processes for SSDS formation, liquefaction and fluidization, governs by various factors, including deformation mechanisms, driving forces, and triggering agents (Owen *et al.* 2011). Liquefaction and fluidization processes are primarily induced by reverse density or gravitational instability (Owen, 1987; Quia *et al.* 1994; Moretti *et al.* (2016). Several significant research in deep-time sediment sequence relates the SSDS with ancient earthquake (*seismite*; Seilacher, 1969). The correlation of SSDS with earthquake magnitude and its relation with maximum distance of liquefaction from earthquake epicentre provide a better understanding of tectonics activity (Silva *et al.* 1997; Vanneste *et al.* 1999; Rodríguez-Pascua *et al.* 2000; Greb and Archer, 2007; Salomon *et al.* 2018; Morsilli *et al.* 2020). Recent investigations have revealed that the formation of SSDS can also be triggered by aseismic forces such as storm waves, tidal shearing, rapid sedimentation and overloading (Quai *et al.* 1994; Moretti and Sabato, 2007; Owen *et al.* 2011; Van Loon and Dechan, 2013; Van Loon and Pisarska-Jamroży, 2014; Jamil *et al.* 2021). Studies exploring the relationship between seismic and aseismic triggers of SSDS suggest that neither the deformation structures nor their characteristics can uniquely identify the triggering agents (Owen *et al.* 2011). The researchers engaged in palaeo-seismicity study propose that seismic deformed beds may exhibit lateral persistence, vertical repetition and change of SSDS morphology in lateral continuity (Seth *et al.* 1990; Montenat *et al.* 2007; VanLoon, 2009; VanLoon and Pisarska-Jamroży, 2014; Owen *et al.* 2011; Quai *et al.* 2013; Zhong *et al.* 2022). However, a number of researchers records these characteristics of SSDS beds in storm- and tide-dominated environments (Alfaro *et al.* 2002; Owen *et al.* 2011; Shanmugam,
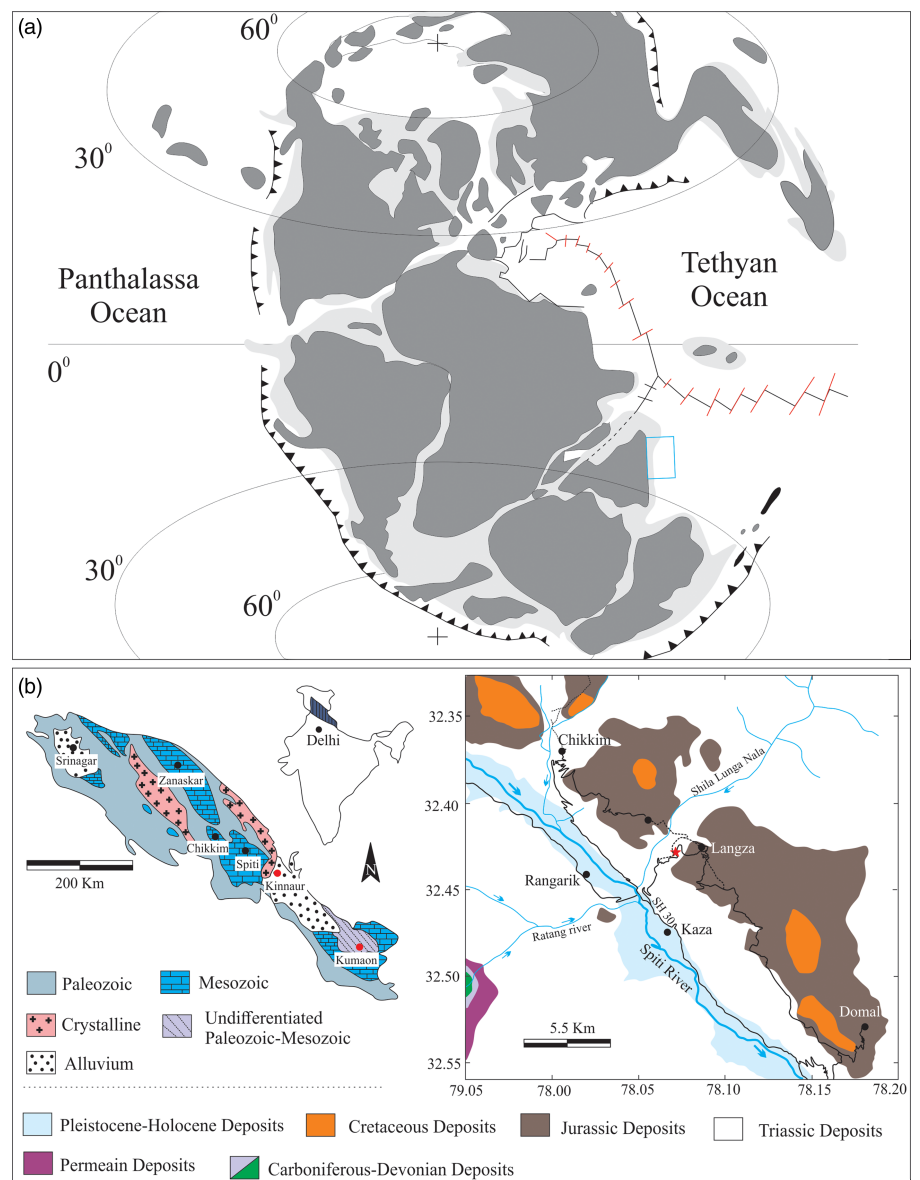
Figure 1. (Colour online) Global paleogeography during Early Jurassic (a, modified from Damborenea, 2002, note the northern boundary of Indian continental margin along Tethys marked by blue rectangle), geological sketch map of Himalaya and position within India (b, map modified after Bhargava and Bassi, 1998). Note the enlarged view of the Spiti region and road map showing location of studied sections, marked by the red stars.

2016 and references therein). Thus, discerning the seismic repercussions within rock sequences, spanning significant geological periods, always presents a formidable task.

On this controversy, recent studies have put forth the proposition that the seismic activity can lead to changes in facies and facies associations (Owen *et al.* 2011; Moretti and Ronchi, 2011; Sarkar *et al.* 2014; Guo *et al.* 2023). Highlighting the importance of comprehending the deformation mechanisms and driving forces involved, a number of studies have documented the change in facies and facies association at onset of *seismite*, such as fluvial to lacustrine (Moretti and Ronchi, 2011), shallow to deep marine (Sarkar *et al.* 2014) and marine to lacustrine (Chen *et al.* 2020; Laborde-Casadaban *et al.* 2021; Yu *et al.* 2022). Despite these findings, there has been limited exploration on the change in facies and facies association for correlating palaeo-seismites. Therefore, the impact of seismic activity on basin palaeoceanography and sedimentation style is poorly constrained.

Here, we focus on the Middle Jurassic succession of Spiti Himalaya, in and around Langza, India, from Ferruginous Oolitic Formation (FOF) to the lower member of Spiti Formation (SF), which was deposited in the southern hemisphere of Tethys along the north-eastern boundary of the Indian plate (Fig. 1). The depositional sequence represents a transition from limestone to anoxic black shale (Bhargava and Singh, 2019; Fursich *et al.* 2021; Albert *et al.* 2021). Several studies focus on the change in palaeoclimate and ocean chemistry (Bhargava and Singh, 2019; Fursich *et al.* 2021; Singh *et al.* 2021), while the cause of facies transition is yet to be explored. The present study records a number of beds with soft-sediment deformations on top of the FOF. The detailed sedimentological study provides insights into the sediment architecture, depositional environment and sea-level fluctuations. The objectives of this study are (a) origin of SSDS, (b) role of seismic *vs.* aseismic processes on the SSDS formation and (c) impact of seismicity on palaeogeographic evolution and sedimentary architecture. The integrated study of facies analysis, characteristics of SSDS and their origin documents the role of seismicity on basin palaeogeographic evolution and sedimentation architecture.

2. Geological setting

The Himalayan sedimentary succession deposited along the north-eastern boundary of India in the southern hemisphere of Tethys holds crucial information on Eocambrian to Eocene (Fig. 2a; Bhargava and Singh, 2019; Fursich *et al.* 2021; Albert *et al.* 2021; Sun *et al.* 2021). The Jurassic succession is mainly preserved at the inner part of the higher Himalayas, often representing the scenario during Gondwana's disintegration. While the Triassic-Jurassic boundary has not been drawn yet, the overall depositional scheme of the Jurassic succession consists of Tangling Formation (TF), FOF and SF, respectively (Bhargava, 2008; Bhargava and Singh, 2019; Fig. 2a). The lithostratigraphic distribution of the Jurassic succession and their respective age is in Table 1. The TF, resting on the Para Formation, consists of the greyish-blue carbonate deposited during Early Jurassic directly transit to FOF with a disconformity in-between (Fig. 2a; Bhargava, 2008; Bhargava and Singh, 2019; Fig. 2a). The FOF consists of alternating beds of oolitic limestone and shale, deposited from Bajocian to Early Callovian (Krishna *et al.* 1982; Bhargava and Singh, 2019 and reference therein; Fig. 2a). The SF is composed predominantly of shale, directly transit from FOF and gradationally passes into the Giumal Formation with sand-shale alternation (Bhargava and Singh, 2019). The lithological variation divided the entire sequence into three major divisions: lower, middle and upper members (Fig. 2a). The fossils constrain Middle Callovian to Late Oxfordian, Kimmeridgian to Early Tithonian, and Early Tithonian to Berriasian age for lower, middle and upper member of SF, respectively (Bhargava and Bassi, 1998; Pandey *et al.* 2013; Singh *et al.* 2021; Fig. 2a; Table 1).

3. Result

3.a. Facies and facies association

The studied sedimentary sequence is dominantly composed of limestone and shale, distinguished as two major parts with laterally persistence-continuous soft-sediment deformation in-between FOF and lower member of SF (Fig. 2b). The lower part of the interval zone is composed of alternate beds of limestone and shale, whereas the upper part consists of thick black shale with occasional calc-arenite beds (Fig. 2b). The lower and upper parts of the SSDS interval identified as facies association I and II, respectively. Although most of the primary sedimentary structures are erased, the preservation of SSDS within limestone suggests that these beds as part of F.A-I. The detailed facies in each facies association is as follows.

3.a.1. Facies Association I: Facies distribution in FOF

The facies association I (F.A-I) represents the FOF of the Kioto Group (Fig. 2a). It is characterized by shallow-water limestone grainstone beds alternating with variable thickness of mud (Fig. 2b). The shale beds mainly consist of planar lamination, while primary sedimentary structures in limestone include massive, hummocky cross-stratified, trough cross-stratification, ripple laminated and planar laminated beds (Fig. 3). The limestone beds consist of abundant broken fragments of fossil invertebrates, with sharp erosional base gradationally transiting to massive, hummocky cross-stratification, trough cross-stratification and ripple laminae (Fig. 3a-d). The hummocky cross-stratification is characterized by series of hummocks and swells, showing erosional contact with planar laminated shale beds (Fig. 3d). The wavelength of hummocks varies from 80 cm to 35 cm. The cross-stratifications

are identified by very low-angle cross-bedding (Fig. 3e). The cross-stratification dips 10°–25° towards NW. The tops of the beds are ripple laminated. The planar laminated limestone at the top of the sequence is dominated by micrite (Fig. 3f). The shale beds are mainly grey in colour, preserving planar laminae (Fig. 3g).

3.a.2. Facies Association II: Facies distribution in lower member of SF

The facies association II (F.A-II) represents the lower member of SF, consisting of a thick shale sequence with occasional calc-arenite beds (Fig. 4a-b). The shale is mainly dark black with few inter-bedding of grey calc-arenite beds (Fig. 4a). This planar laminated shale is intervened by calc-arenite beds with sharp and erosional scour base (Fig. 4c). The massive beds show haphazard orientation of fossils like belemnite and bivalves (Fig. 4c). The calc-arenite beds are massive in places, with a thickness varying from 10 to 25 cm. These beds are composed of micrite with abundance belemnite fossils (Fig. 4c-d). The massive beds are graded to ripple lamination in places (Fig. 4d). The planar laminated dark shale shows bed-parallel orientation of belemnites (Fig. 4d).

3.b. Characteristics of SSDS

The studied sediment sequence preserves the SSDS at the topmost part of FOF (Fig. 2b). The SSDS beds are composed of fine- to medium-grained carbonate, which are overlain and underlain by shale. The SSDS beds have appeared four times in the stratigraphic sequence, which were documented in two sections (Fig. 2b; Fig. 5a). The SSDS displays a wide range of scale and geometry. The SSDS are mainly syn-sedimentary faults, insitu breccia, load casts and ball-pillow structures (Fig. 5b-f; 6). Detailed description of SSDS are as follows.

Syn-sedimentary faults: Small-scale faults, which vertically transit to normal depositional laminae, are prevalent features within sediment sequences. They predominantly manifest as high-angle normal faults (Fig. 5b), occasionally exhibiting reverse faulting. The fault offsets typically range from a few cm to around 15 cm. These faults are present in a series of sub-parallel flexure associated with slide planes (Fig. 5c). The pole plots of these faults show two prominent orientations: one trending towards the northwest and the other towards the southeast (Fig. 5c). This layer is overlain by undeformed planar laminated shale (Fig. 5b, c). Furthermore, these faults commonly coincide with faulted breccia.

Load casts: Load casts are recognized in heterolithic succession at the interface between carbonate and shale bed (Fig. 5d). They display flat tops and irregular concave up base (Fig. 5d, e). Load structures show slight to deep penetration into the underlying shale layer and range in depth from few cm to 15 cm. Few structures show single loads, while many of them display multiple load collages (Fig. 5e). The multi-loads are asymmetric in fashion. The single and multi-load structures are associated with flame structures (Fig. 5e). The overall thickness of the bed is 40 cm, which shows a massive appearance.

Ball and Pillow structures: The ball and pillow structures occur within limestone-shale inter-bedding (Fig. 5f). The thickness of this deformed bed is about 45 cm. The deformed bed exhibits isolated ball- and pillow-like structures. Entire bed shows detached ball and pillow features and trace of original laminae is rarely preserved. The maximum diameter of ball/pillow is around 30 cm.

Faulted breccia: The breccia consists of irregular, sub-angular to angular carbonate clasts suspended within a matrix of mudstone (Fig. 6a-b). The clasts exhibit a predominantly random orientation,
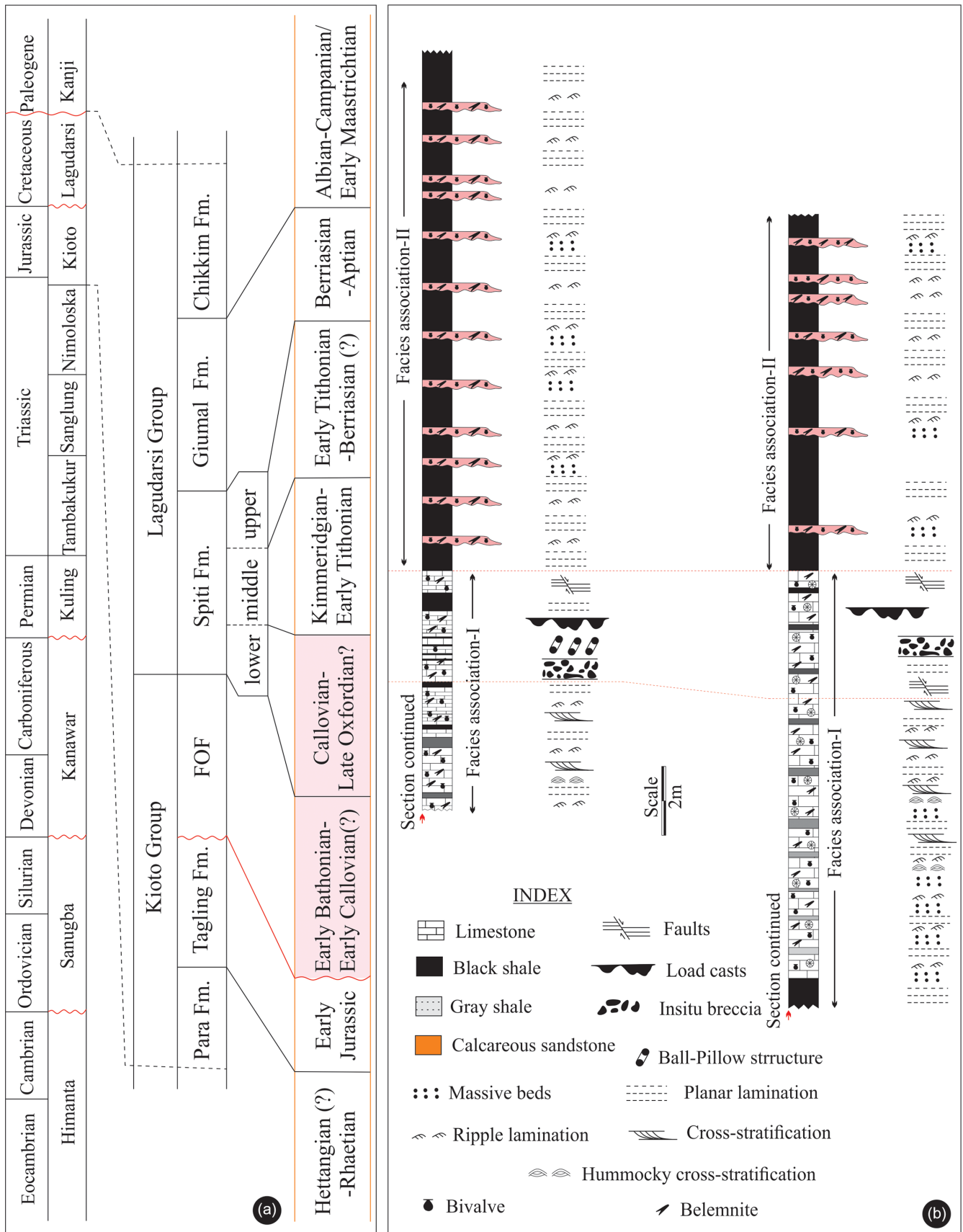
Figure 2. (Colour online) Lithostratigraphy and biostratigraphy distribution in parts of Spiti Himalaya sequence (a, note the age of studied succession marked by pink color), lithological log in two best locations from FOF to lower member of SF (b, note the SSDS zone at top part of FOF, distance from one section to another section ~1 km).

Table 1. Lithostratigraphy and age of Jurassic sediment succession (Modified after Fursich *et al.* 2021)

Lithostratigraphy		Description	Age
Giumal Formation		–Glauconitic sandstone and siltstone. –Few bivalves.	Albian-Berriasian
Spiti Formation	Upper Member	–Shaly argillaceous silt and common thin siltstone beds. –Fossils comparatively rare.	Berriasian?-Early Tithonian
	Middle Member	–Shaly argillaceous silt with abundant concretions and occasional thin sandstone intercalations. –Common ammonites.	Early Tithonian-Kimmeridgian
	Lower Member	–Shaly argillaceous silt. –Abundant belemnites and common bivalves.	Late Oxfordian to Middle Callovian
Ferruginous Oolitic Formation		–Cross-bedded sandstone, siltstone and limestone. –Some beds have ferruginous ooids. –Occasional belemnites concretion.	Early Callovian-Early Bathonian
Tagling and Para Formation		–Well cemented thick-bedded limestone. –Hardground with encrusting oysters near top. –Common shell fragment	Middle Jurassic?-Late Triassic

varying in length from ~2 cm to very large (up to 1 m). The larger breccia clasts display a distinctive rectangular shape, retaining remnants of the original bedding and lamination, providing clues to their source (Fig. 6a-b). The jagged boundaries of clasts show interlocking relationship, revealing the original bedding patterns, which often become disrupted along faulted boundaries (Fig. 6a-b). The average thickness of breccia bed is ca. 1.5 m. This bed occurs on the undeformed limestone and is covered by thin (~5 cm) shale bed.

4. Discussion

4.a. Depositional environment and Palaeobathymetry

The studied sections of Jurassic Spiti Himalaya consist of two facies association with soft-sediment deformation beds at their respective interval. The deformed beds rest on F.A-I and are composed of alternative carbonate and shale beds. The presence of massive beds, hummocky cross-stratification and cross-stratification within the limestone indicate high-energy flow. The transition of massive bed to ripple lamination through hummocky cross-stratification within a single bed infers a waning flow. The sharp erosional base of the limestone also supports the high-energy storm. The ripple laminated limestone may have been deposited in the waning flow of storm or wave influence. The deposition of shale and carbonate in the same environment infers depositional condition was fluctuating abruptly. Considering the underlying thick carbonate sequence of Tagling Formation, we infer the depositional environment within the storm-dominating middle shelf setting.

The dominance of black shale with occasional calc-arenite beds in F.A-II suggests greater depth than the F.A-I, where the planar laminated shale deposited from suspension falls out in a calm and quiet environment. The earlier studies on palaeoredox suggested that the depositional site was dysoxic-anoxic (Fursich *et al.* 2021; Albert *et al.* 2021). The absence of coarse-grained sediment in an anoxic zone infers depositional site below the wave and storm base. In the absence of wave and storm, the sharp scour base of massive calc-arenite beds suggests that these are the deposits of slope failure or turbidite (Bouma, 1962; Shanmugam, 2021). These massive beds may also be related to hybrid beds like turbidites-debrite couplets (Jamil *et al.* 2021). The development of hybrid

beds is highly influenced by frontal and lateral lobe settings. The frontal lobes initially deposit coarse sandstones, which is followed by the gradual evolution of flow conditions (Jamil *et al.* 2021). The haphazard orientation of fossils in the massive bed also supports the context of rapid sedimentation. The thin ripple lamination on massive beds may be related to the spreading of sediments in lateral lobes starting from an off-axis area that provides a small avenue for the transition of flow and the deposition of hybrid beds (Davis *et al.* 2009; Fonnesu *et al.* 2016, 2018; Jamil *et al.* 2021). In general, progradation of hydride bed movement in deep-sea progress on the erosional surface (Hofstra *et al.* 2016; Kane *et al.* 2017; Jamil *et al.* 2021). Considering the thick black shale deposits, we infer that F.A-II is deposition of deep marine, outer shelf.

4.b. Origin of SSDS: Seismic vs. Aseismic triggering processes

The studied sequence consists of shale-limestone repository (F.A-I) and thick black shale (F.A-II), with laterally extended four repetitive SSDS beds on top of the F.A-I (Fig. 2b, 5a). The SSDS include syn-sedimentary faults, load casts, ball-pillow structures and insitu breccia. Each of these deformed beds are overlain and underlain by the undeformed beds. The syn-sedimentary faults, load casts, and insitu breccia occur in both the studied sections, while ball and pillow structure is observed in one of the sections.

SSDS form in unlithified sediments during or soon after deposition, exhibit plastic and/or brittle deformations (Owen, 1987; Moretti and Sabato, 2007). The deformation mechanism enables to overcome the yield strength of solid materials, which temporally behave like a liquid manner and deform as a viscous fluid (Owen, 1987), ultimately resulting the liquefaction and fluidization. Liquefaction and fluidization processes obscure the primary lamination and fabric of the sediment deposits (Obermeier, 1996). The driving forces responsible for the SSDS include gravitational body forces, unstable density gradients, shear stresses, and unevenly distributed loads, reflecting the SSDS morphology (Owen, 1987).

4.b.1. Deformation mechanism and driving force

The deformation mechanism classifies the distribution of SSDS in the studied succession into two groups: liquefied and fluidized structures (load casts, ball-pillow structures) and plastic or brittle
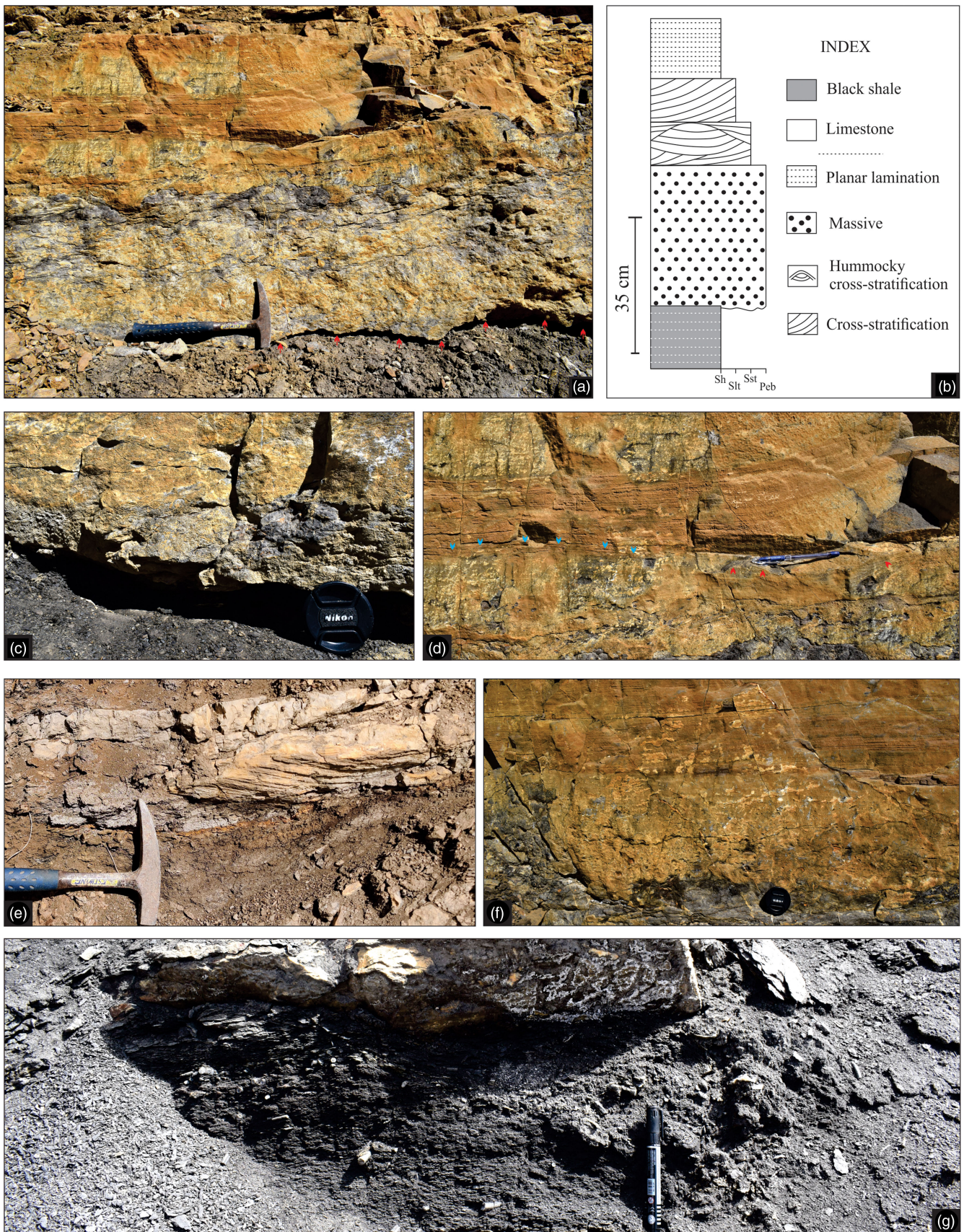
Figure 3. (Colour online) Facies distribution in FOF (Facies association-I): a single limestone bed preserved massive character, hummocky cross-stratification and planar lamination in ascending order with sharp, scour base on shale (a, hammer length 35 cm, note scour base marked by red arrows), sketch of Fig. 6a (b), abundant fossils in massive bed with sharp scour base (c, camera cover diameter 5 cm), hummocks and swales are marked by blue and red arrows respectively (d, pen length 15 cm), cross-stratified limestone with sharp, erosional base (e, hammer length 35 cm), planar laminated limestone facies (f, camera cover diameter 5 cm), alternating shale and limestone beds (g, marker length 15 cm).
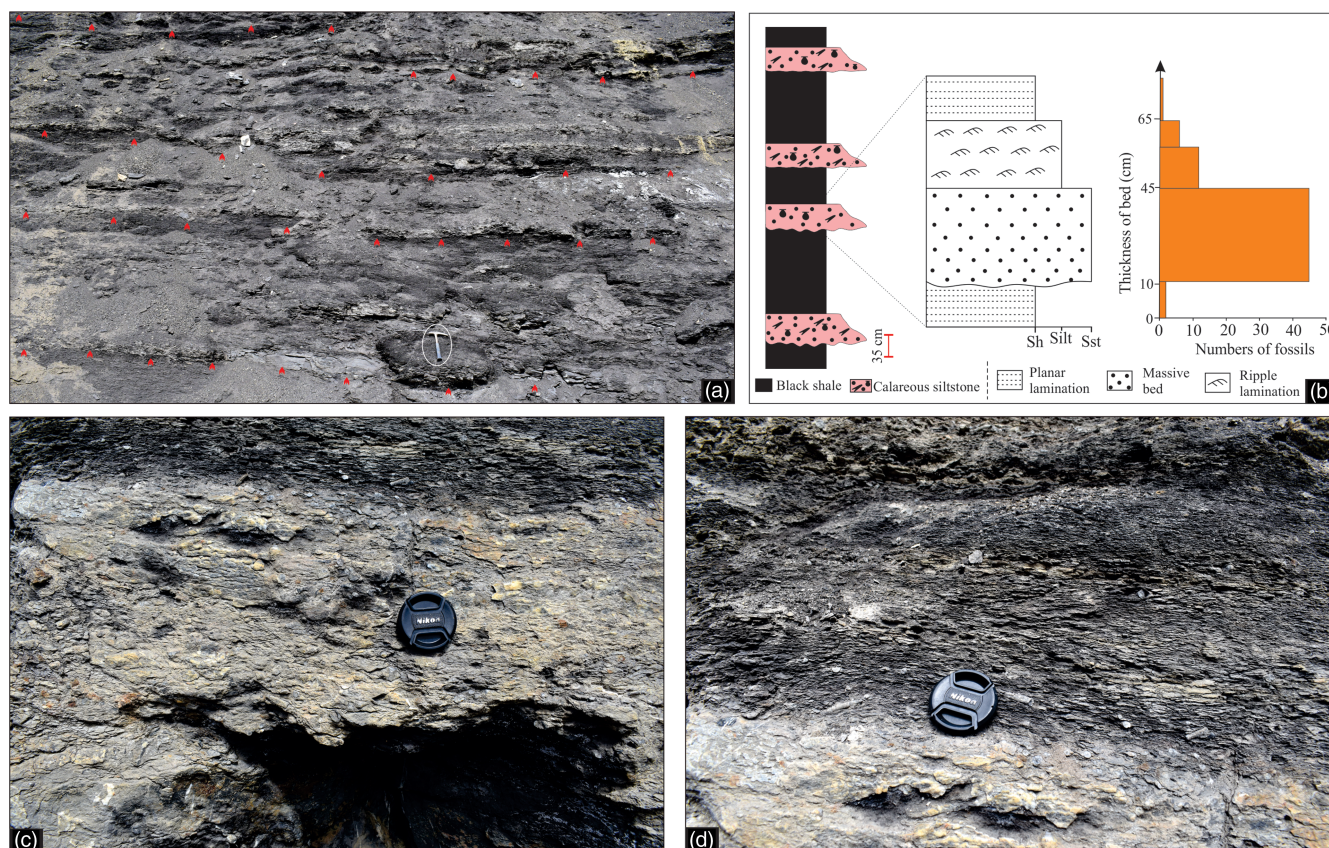
Figure 4. (Colour online) Facies distribution in lower member of SF (Facies association-II): thick shale sequence with occasional calc-arenite beds (a, hammer length 35 cm, note the sharp, erosional base of calcareous beds are marked by arrows), log of Fig. 4a and primary sedimentary structures distribution in association of calcareous bed (b, note count of fossils), massive bed with sharp, scour base (c, lens cover diameter 5 cm), ripple laminated and planar laminated shale (d, lens cover diameter 5 cm).

deformation (syn-sedimentary faults and insitu breccia). The deposition of high-density limestone bed on low-density muds created an inverted density gradient (Anketell *et al.* 1970; Owen, 1987; Quai *et al.* 1994; Owen *et al.* 2011). The liquefaction induced by the unstable density at the limestone-shale interface formed the load structures (Owen, 1987). In a similar fashion, in the joint action of density gradient and gravity instability, liquefaction and fluidization of underlying beds leads to the formation of the ball-pillow by the separation of the loads (Moretti *et al.* 2001; Quai *et al.* 2013). The alignment of flames along a specific direction suggests strong shear force direction. Ball and pillow structures commonly form by the liquefaction-fluidization processes, triggered by seismic shocks (Owen, 1996; Molina *et al.* 1998; Moretti *et al.* 1999; Tian Hongshui *et al.* 2016a, b; Zhong *et al.* 2019).

Syn-sedimentary faulting in limestone beds demonstrates brittle behaviour, as indicated by the discontinuities caused by faulting in alternating beds of mud and sand (Owen, 1987). The inclined micro-fault blocks exhibit a parallel stair-step pattern, which reflects the influence of gravitational forces (specifically lateral stress) and/ or slumping on the deformation process (Salomon *et al.* 2018). During the slump initiation, layer-parallel normal and reverse faults form at the head and toe of the slump, respectively (Salomon *et al.* 2018). The fluidization pressure during deformation damaged the harder limestone beds and formed breccia (Quai *et al.* 1994; Yu *et al.* 2022). The semi-plastic deformation mechanism of the shale and limestone layers forms breccia.

4.b.2. Argument of seismic vs. aseismic origin

Furthermore, although both brittle-ductile deformation and liquefaction/fluidization contribute to the studied SSDS, analysis of the triggering agents in marine settings indicates that these structures can form due to sediment overloading (Allen, 1982; Moretti *et al.* 2001; Moretti and Sabato, 2007), tidal shear (Tessier and Terwindt, 1994; Greb and Archer, 2007), tsunamis (Takashimizu and Masuda, 2000; Nanayama *et al.* 2000; Schnyder *et al.* 2005; Le Roux *et al.* 2008), wave-storm pounding (Molina *et al.* 1998) and seismic shocks (Sim, 1975; Owen *et al.* 2011; Moretti and Ronchi, 2011; Sarkar *et al.* 2014; He and Qiao, 2015). The preservation of undeformed beds on top of SSDS beds suggests that deformation must have been triggered at the sediment-water interface; otherwise, liquefaction and fluidization would have affected the overlying beds (Owen, 1996). This discounts the possibility of overloading as the main trigger. The tidal shearing also can form a similar type of SSDS via storm pounding-induced liquefaction and fluidization, but the absence of any tidal signal in the depositional site also discards the tidal shearing effect. The dominance of wave and storm signatures in the depositional environment argues as a possible triggering agent. However, the confinement of the SSDS layer at the topmost part of the FOF infers that seismicity must have triggered deformation. We interpret the soft sediment deformation structures in the Jurassic succession of Spiti Himalaya as *seismite*. The seismicity favours capturing lateral continuity of the deformation structures over several hundred metres, vertical repetition, and change of facies assemblages from
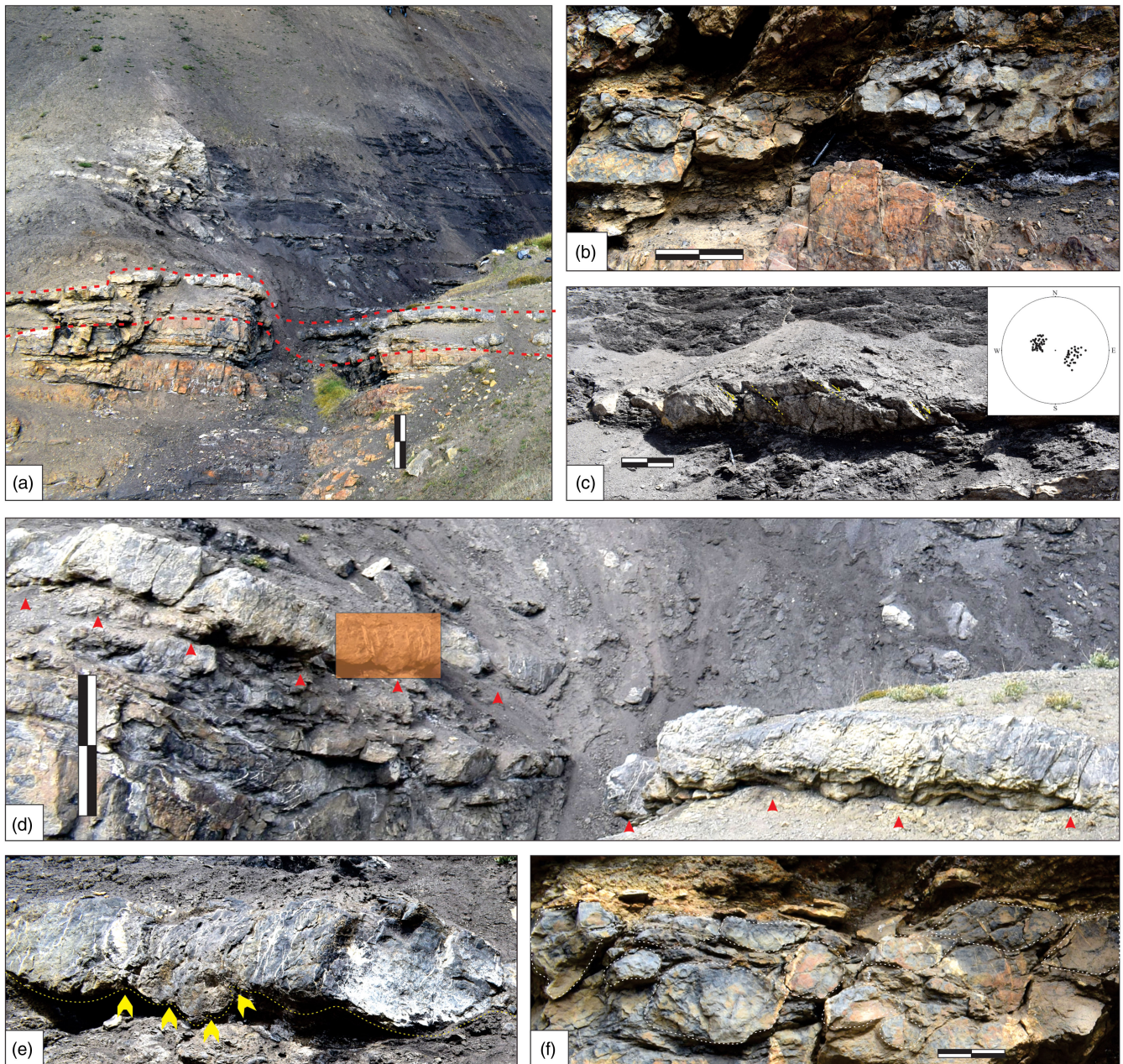
Figure 5. (Colour online) Soft-sediment deformation structures zone in studied section(a, bar length 5m; note the SSDS zone marked by red dotted line), syn-sedimentary faults (b, bar length 30 cm); abundance slide planes at the fault plane (c, bar length 30 cm, note the pole of slide inset), laterally continuous load cast bed (d, bar length 1m; note the loads are protruded in underlying shale layer; see asymmetric load in inset); enlarge view of load casts marked by yellow rectangle in Fig. 5d (e, note flame structures are marked by yellow arrow), ball-pillow structures (f, bar length 15cm; ball structures are marked by white dotted lines).

F.A-I to II (Owen *et al.* 2011; Moretti and Ronchi, 2011; Sarkar *et al.* 2014; He *et al.* 2014; Chen *et al.* 2020; Guo *et al.* 2023).

4.c. Relationship of the seismicity and SSDS: Magnitude of Earthquake

While the differential liquefaction and fluidization is the main agent to form the soft-sediment deformation, the final morphology of SSDS is controlled by the driving force. SSDS not only identify the palaeo-seismite but also measure the earthquake magnitude and faulting activity (Quia *et al.* 2013; He *et al.* 2014, 2015; Zhong *et al.* 2022). The SSDS in the studied sediment sequence provide

the intensity of palaeo-earthquake as well (Allen, 1986; Rodríguez-Pascua *et al.* 2000). Some authors stated that intensity of an earthquake greater than 5 (M≥5) can produce liquefaction and fluidization (Atkinson, 1984; Audemard and De Santis, 1991; Galli, 2000; Wheeler, 2002; Zhong, 2017; Zhong *et al.* 2022; Guo *et al.* 2023). The computer modelling suggests M≈5 produce liquefaction feature within 4 km radius of the earthquake epicentre (Atkinson, 1984), but a few studied debates on M≈4.5, M≈5.5, and M≈7 for liquefaction and fluidization structures depending on the grain size (Marco and Agnon, 1995; Ambraseys, 1988; Obermeier, 1996). The preservation of load casts, ball-pillow structures indicates that the studied sediment was affected by at
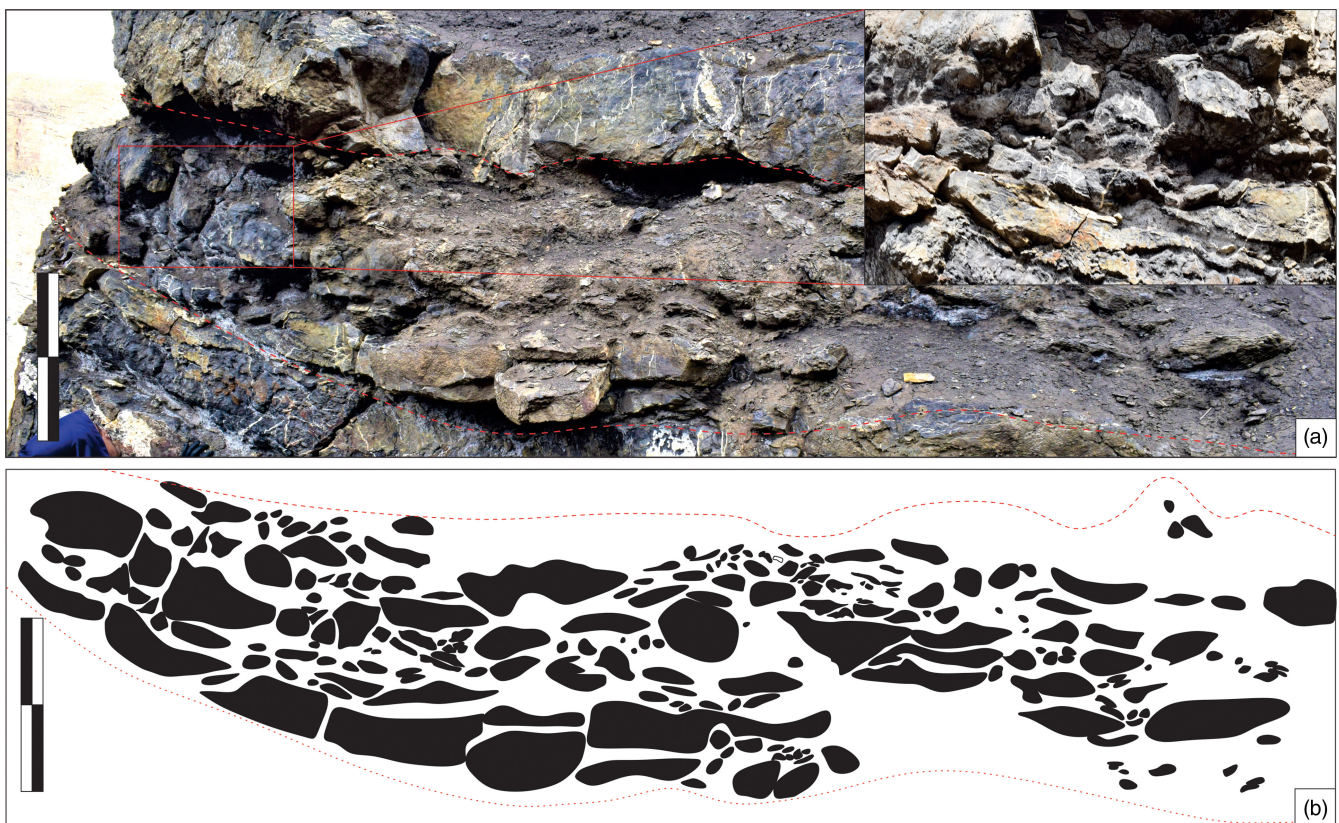
Figure 6. (Colour online) Soft-sediment deformation structure: insitu breccia (a, bar length 1 m; enlarge view in inset); sketch of insitu breccia bed (b).

least an earthquake magnitude of 5.0–7.0 (Rodríguez-Pascua *et al.* 2000). SSDS in four repetitive beds suggests the sediment succession may have affected four seismic pulses.

4.d. Response of basin on seismic impact: Carbonate shelf to black shale transition

The vertical transition from F.A-I to F.A-II provides clear evidence of a distinct shift from a mixed siliciclastic (shale)-carbonate repository to black shale. The overall increase of mud and absence of carbonate in the F.A-II sequence define the demise of carbonate platform (Fig. 7a). Increasing mud and the disappearance of carbonate suggest that the depositional site may have entered below the photic zone via transgression (Fig. 7a). The onset of sea-level rise is marked by the change from mixed carbonate repository to black shale. The occurrence of the *seismite* at the junction between two contrasting depositional setups suggests the role of seismicity on the environmental change. The facies immediately overlying on the *seismites* represent the deepest among all facies associations, implying a rapid rise in relative sea level to its maximum extent. This rapid transgression is defined as an event of basin subsidence, including the formation of syn-sedimentary faults and breccia. This subsidence resulted in a sudden shift from the middle to the outer shelf, evident through carbonate setback and thick anoxic black shale (Fig. 7b-c). The regional distribution of the SSDS, coupled with the evidence of a sudden and sharp increase in sea level, can only be satisfactorily explained by intense tectonic activity, including earthquakes that deformed the sedimentary layers at the surface, leading to rapid basin subsidence (Fig. 7b-c; He *et al.* 2014; Sarkar

et al. 2014). It is important to note that sediment supply remained low during this period, resulting in the dominance of fine-grained suspension fall-out and the absence of coarse sediment in the depositional site. The abrupt palaeogeographic changes, observed during the onset of *seismites,* are further supported by turbidity flows. The occurrence of turbidites in F.A-II suggests that the tectonic subsidence may have created some slopes, along which calc-arenite beds were transported from shallow-water environments and preserved in the deep marine setting (Fig. 7c). The significant positive shift observed across the *seismite* interval provides additional force for the water-level rise and develops anoxic conditions, leading to sedimentation (Fig. 7c).

4.e. Implication in region study and global perspective

The records of seismite in the studied Jurassic succession indicate the occurrence of palaeo-seismic belt close to the depositional setting (Quai *et al.* 2013). The seismic impact subsided the basin and caused the transition of the depositional environment from mixed siliciclastic-carbonate repository to anoxic black shale. The rapid subsidence increased the sea level without affecting the eustatic sea level (Moretti and Roonchi, 2011; Sarkar *et al.* 2014; He *et al.* 2014). On the deformed Himalayan belt, the basin-wide correlation of sedimentary succession is always challenging. However, the seismite at the boundary between FOF and the lower member of SF is very useful for the stratigraphic correlation. The seismic pulses often directly correlate with the convergence and divergence of plates (Chen *et al.* 2020; Laborde-Casadaban *et al.* 2021; Mueller *et al.* 2023). Considering
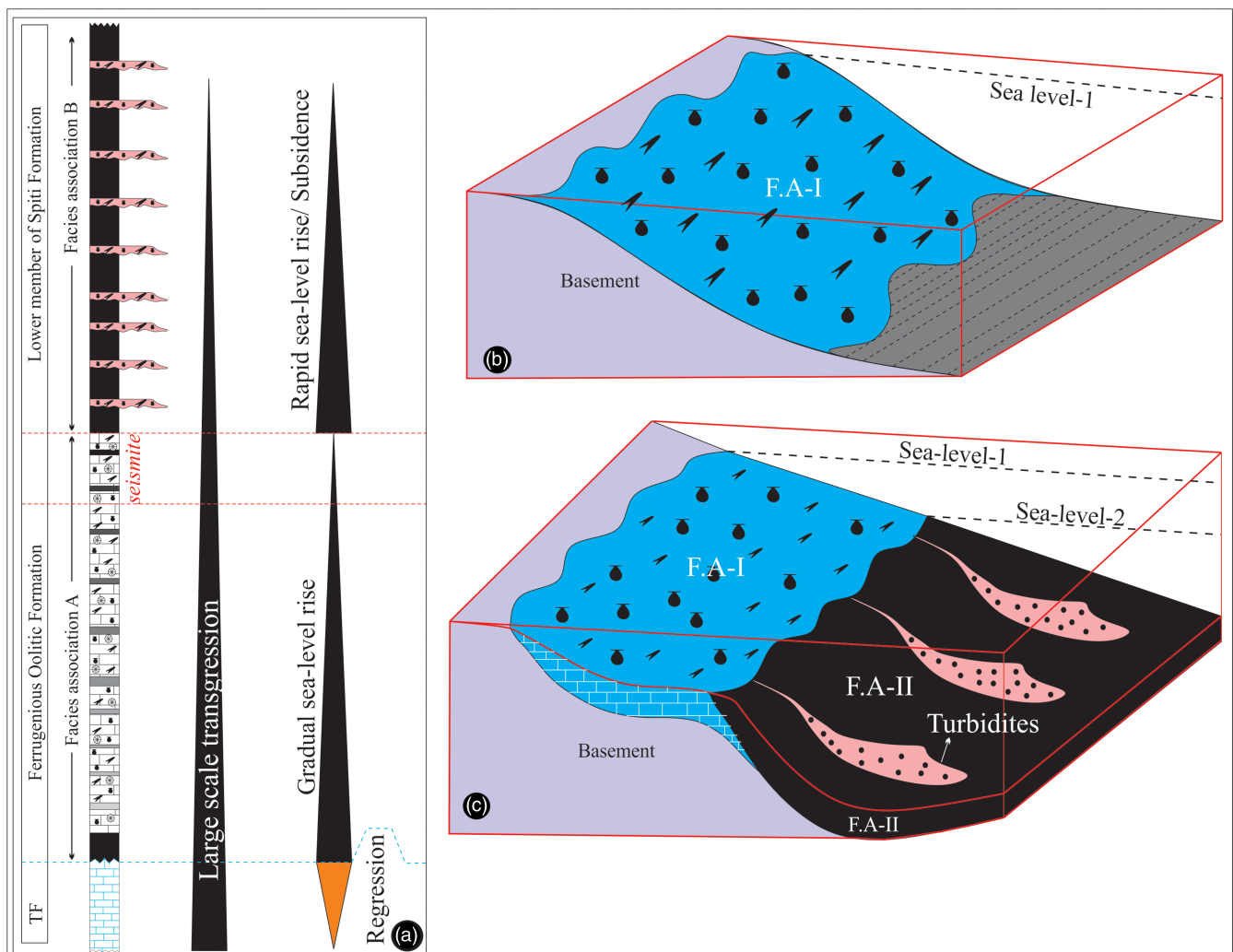
Figure 7. (Colour online) Conceptual model: vertical section showing F.A-I passes upward to F.A-II with a seismite layer at the top of F.A-I (a, note fining up sequence and transgression-regression cycle), depositional scenarios for F.A-I (b, note the sea level-1), depositional scenarios for F.A-II (c, note sea level-2 provoked by seismicity induced subsidence).

the Middle Jurassic Tethys sea-floor deposition, we infer that the Middle Jurassic Gondwana breakup and synchronous active rifting (Lovecchio *et al.* 2020) may be linked to the studied seismic pulses.

The seismite in the present study includes the impact of seismicity across the basin and is associated with a change in the palaeogeography, which is reflected in facies distribution and sedimentation architecture. Therefore, the sedimentological study should be the key for the identification of seismite for basin-wide correlation.

5. Conclusions

Considering the SSDS distribution and sediment dynamics pattern at onset of the SSDS beds, we draw the following conclusion.

(a) Laterally persistent four repetitive deformed beds at the topmost part of FOF result from the seismic impact. The liquefaction and fluidization were induced by reverse

density/ gravity instability (for load casts, and ball-pillow structures) and plastic or brittle deformation (syn-sedimentary faults and insitu breccia) provoked by seismic shocks.

(b) The dominance of strong waves and storm in the depositional site argue against the seismic impact, while the sharp change of facies distribution interprets seismicity is the only possibility. Recurrence of SSDS beds at four intervals suggests that the depositional site was affected by earthquake at least four times. The association of SSDS features indicates moderate to strong magnitude earthquakes.

(c) The seismic impact rapidly subsided the basin, which increased the sea level. Basin subsidence caused the shift of the depositional environment from middle shelf to outer shelf. Further, the deepening of basin with climatic calamity enhanced anoxicity, causing transition from carbonate-shale repository to black shale deposition.

(d) The seismite beds may be useful for the stratigraphic correlation, demarcating the boundary between FOF and SF along the palaeo-Tethyan coast of India. The Gondwana breakup during Middle Jurassic and related rifting may be

References

Alberti M, Fürsich TF, Pandey DK, Andersen N, Garbe-Schönberg D, Bhosale S, Chaskar K and Habermann JM (2021) First record of stable isotopes (δ13C, δ18O) and element ratios (Mg/Ca, Sr/Ca) of Middle to Late Jurassic belemnites from the Indian Himalayas and their potential for palaeo-environmental reconstructions. *Journal of Paleogeography* **10**, 1–22.

Alfaro P, Delgado J, Estévez A, Molina JM, Moretti M and Soria JM (2002) Liquefaction and fluidization structures in Messinian storm deposits (Bajo Segura Basin, Betic Cordillera, southern Spain). *International Journal of Earth Sciences* **91**, 505–513.

Allen JRL (1982) *Sedimentary Structures, their Character and Physical Basis.* New York: Development in Sedimentology, Elsevier.

Allen JRL (1986) Earthquake magnitude-frequency, epicentral distance, and soft-sediment deformation in sedimentary basins. *Sedimentary Geology* **46**, 67–75.

Ambraseys N (1988) Engineering seismology. *Earthquake Engineering and Structural Dynamics* **17**, 1–105.

Anketell JM, Cegla J and Dzulynski S (1970) On the deformational structures in systems with reversed density gradients. *Annales de la Societe Geologique Pologne* **40**, 3–30.

Atkinson G (1984) Simple computation of liquefaction probability for seismic hazard applications. *Earthquake Spectra* **1**, 107–123.

Audemard FA and de Santis F (1991) Survey of liquefaction structures induced by recent moderate earthquakes. *Bulletin of the International Association of Engineering Geologists* **44**, 5–16.

Bhargava ON (2008) An updated introduction to the Spiti geology. *Journal of Palaeontological Society of India* **53**, 113–129.

Bhargava ON and Bassi UK (1998) Geology of the Spiti-Kinnaur, Himachal Himalaya. *Memoirs of the Geological Survey of India* **124**, 1–210.

Bhargava ON and Singh BP (2019) Geological evolution of the Tethys Himalaya. *Episodes* **43**, 404–416.

Bouma AH (1962) *Sedimentology of Some Flysch Deposits.* Amsterdam: Elsevier. 169 p.

Chen A, Zhong Y, Ogg JG, van Loon AJ, Chen H, Yang S, Liu L and Xu S (2020) Traces of the Triassic collision between the North and South China blocks in the form of seismites and other event layers. *Journal of Geodynamics* **136**, 1–16.

Damborenea SE (2002) Jurassic evolution of Southern Hemisphere marine palaeobiogeographic units based on benthonic bivalves. Geobios 35, Mémorial Special **24**, 51–71

Davis C, Haughton P, McCaffrey W, Scott E, Hogg N and Kitching D (2009) Character and distribution of hybrid sediment gravity flow deposits from the outer Forties Fan, Palaeocene Central North Sea, UKCS. *Mararine and Petroleum Geology* **26**, 1919–1939.

Fonnesu M, Felletti F, Haughton PDW, Patacci M and McCaffrey WD (2018) Hybrid event bed character and distribution linked to turbidite system sub-environments: The North Apennine Gottero Sandstone (north-west Italy). *Sedimentology* **65**, 151–190.

Fonnesu M, Patacci M, Haughton PDW, Felletti F and McCaffrey WD (2016) Hybrid Event Beds Generated By Local Substrate Delamination on A Confined-Basin Floor. *Journal of Sedimentary Research* **86**, 929–943.

Fürsich FT, Alberti M, Pandey DK, Chasker K and Bhosale S (2021) Facies analysis and palaeoecology of the Jurassic Spiti Shale Formation in the Spiti area, northern India. *Journal of Paleogeography* **10**, 438–462.

Galli P (2000) New empirical relationships between magnitude and distance for liquefaction. *Tectonophysics* **324**, 169–187.

Greb SF and Archer AW (2007) Soft-sediment deformation produced by tides in a meizoseismic area, Turnagain Arm, Alaska. *Geology* **35**, 435–438.

Guo L, He Z and Li L (2023) Lacustrine sedimentary responses to earthquakes —soft-sediment deformation structures since late Pleistocene: A review of current understanding. *Earthquake Research Advances* **3**, 1–8.

He BZ and Qiao X (2015) Advances and overview of the study on paleo-earthquake events: a review of seismites. *Acta Geological Sinica* (English edition) **89**, 47.

He BZ, Quia XF, Jiao CL, Xu ZQ, Cai ZH, Guo XP and Zhang YL (2014) Paleo-earthquake events during the late Early Paleozoic in the central Tarim Basin (NW China): evidence from deep drilling cores. *Geologos* **20**, 105–123.

He BZ, Quia XF, Zhang YL, Tian HS, Cai ZH, Chen SQ and Zhang YX (2015) Soft-sediment deformation structures in the Cretaceous Zhucheng depression, Shandong Province, East China; their character, deformation timing and tectonics implication. *Journal of Asian Earth Science* **110**, 101–122.

Hofstra M, Pontén ASM, Peakall J, Flint SS, Nair KN and Hodgson DM (2016) The impact of fine-scale reservoir geometries on streamline flow patterns in submarine lobe deposits using outcrop analogues from the Karoo Basin. *Petroleum Geoscience* **23**, 159–176.

Hongshui T, Van Loon AJ, Hailin W, Shenhe Z and Jiewang Z (2016a) Seismites in the Dasheng group: new evidence of strong tectonic and earthquake activities of the Tanlu fault zone. *Science China Earth Sciences* **59**, 601–618.

Jamil M, Siddiqui NA, Umar M, Usman M, Ahmed N, Rahman AHA and Zaidi FK (2021) Aseismic and seismic impact on development of soft-sediment deformation structures in deep-marine sand-shaly Crocker fan in Sabah, NW Borneo. *Journal of King Saud University – Science* **33**, 1–13.

Kane IA, Pontén ASM, Vangdal B, Eggenhuisen JT, Hodgson DM and Spychala YT (2017) The stratigraphic record and processes of turbidity current transformation across deep-marine lobes. *Sedimentology* **64**, 1236–1273.

Krishna J, Kumar S and Singh IB (1982) Ammonoid stratigraphy of the Spiti Shale (Upper Jurassic), Tethys Himalaya, India. *Neues Jahrbuch für Geologie und Paläontologie, Monatshefte* **10**, 580–592.

Laborde-Casadaban M, Homberg C, Schnyder J, Borderie S and Raine R (2021) Do soft sediment deformations in the Late Triassic and Early Jurassic of the UK record seismic activity during the break-up of Pangea? *Proceedings of the Geologists' Association* **132**, 688–701.

Le Roux JP, Nielsen SN, Kemnitz H and Henriquez Á (2008) A Pliocene mega-tsunami deposit and associated features in the Ranquil Formation, Southern Chile. *Sedimentary Geology* **203**, 164–180.

Lovecchioa JP, Rohaisb S, Josephb P, Bolattia ND and Ramos VA (2020) Mesozoic rifting evolution of SW Gondwana: A poly-phased, subductionre-lated, extensional history responsible for basin formation along the Argentinean Atlantic margin. *Earth-Science Reviews* **203**, 1–22. https:// doi.org/10.1016/j.earscirev.2020.103138

Marco S and Agnon A (1995) Prehistoric earthquake deformations near Masada, Dead Sea graben. *Geology* **23**, 695–698.

Molina JM, Alfaro P and Moretti M (1998) Soft-sediment deformation structures induced by cyclic stress of storm-waves in tempestites (Miocene, Guadalquivir Basin, Spain). *Terra Nova* **10**, 145–150.

Montenat C, Barrier P, Ott d'Estevou P and Hibsch C (2007) Seismites: An attempt at critical analysis and classification. *Sedimentary Geology* **196**, 5–30.

Moretti M, Alfaro P, Caselles O and Canas JA (1999) Modelling seismites with a digital shaking table. *Tectonophysics* **304**, 369–383.

Moretti M, Alfaro P and Owen G (2016) The environmental significance of soft-sedimentdeformation structures: key signatures for sedimentary and tectonic processes. *Sedimentary Geology* **344**, 1–4.

Moretti M and Ronchi A (2011) Liquefaction features interpreted as seismites in the Pleistocene fluvio-lacustrine deposits of the Neuquén Basin (Northern Patagonia). *Sedimentary Geology* **235**, 200–209.

Moretti M and Sabato L (2007) Recognition of trigger mechanisms for soft-sediment deformation in the Pleistocene lacustrine deposits of the

Sant'Arcangelo Basin (southern Italy): seismic shock vs. overloading. *Sedimentary Geology* **196**, 31–45.

Moretti, M., Soria, J. M., Alfaro, P. and Walsh, N. (2001) Asymmetrical soft-sediment deformation structures triggered by rapid sedimentation in turbiditic deposits. *Facies* **44**, 283–294.

Morsilli M, Giona Bucci M, Gliozzi E, Lisco S and Moretti M (2020) Sedimentary features influencing the occurrence and spatial variability of seismites (late Messinian, Gargano promontory, southern Italy). *Sedimentary Geology* **401**, 1–17.

Mueller P, Tamburelli S, Menegoni N, Perozzo M, Amadori C, Crispini L, Federico L, Seno S and Maino M (2023) Concurrence of load-and-flame structures, balls-and-pillows, clastic injectites and shear deformation bands as indicator of seismicity in mixed siliciclastic-carbonate successions (Finale Ligure Basin, Italy). *Marine and Petroleum Geology* **155**, 1–22. https://doi.org/10.1016/j.marpetgeo.2023.106345

Nanayama F, Shigeno K, Satake K, Shimokawa K, Koitabashi S, Miyasaka S and Ishii M (2000) Sedimentary differences between the 1993 Hokkaido-nansei-oki tsunami and the 1959 Miyakojima typhoon at Taisei, Southwestern Hokkaido, Northern Japan. *Sedimentary Geology* **135**, 255–264.

Obermeier SF (1996) Use of liquefaction-induced features for paleoseismic analysis-An overview of how seismic liquefaction features can be distinguished from other features and how their regional distribution and properties of source sediment can be used to infer the location and strength of Holocene paleo-earthquakes. *Engineering Geology* **44**, 1–76.

Owen G (1996) Experimental soft-sediment deformation: Structures formed by the liquefaction of unconsolidated sands and some ancient examples. *Sedimentology* **43**, 279–293.

Owen G (1987) Deformation processes in unconsolidated sands. In *Deformation of sediments and sedimentary rocks* (eds ME Jones and RMF Preston), pp. 11–24. London, UK: Geological Society of London, Special Publication no. 29.

Owen G, Moretti M and Alfaro P (2011) Recognizing triggers for soft-sediment deformation: Current understanding and future directions. *Sedimentary Geology* **235**, 133–140.

Pandey B, Pathak DB and Krishna J (2013) Preliminary remarks on new ammonoid collection from freshly exposed succession of the Spiti Formation between Lidang and Giumal, Spiti Valley, Himachal Himalaya, India. *Himalayan Geology* **34**, 124–134.

Quia XF and Guo XP (2013) Early Jurassic soft-sediment deformation interpreted as seismites in the Wuqia pull-apart basin and the strike-slip Talas-Ferghana fault, Xinjiang, China. *Acta Geological Sinica* **87**, 730–737.

Quia XF, Song TR, Gao LZ, Peng Y, Li HB, Gao M, Song B and Zhang QD (1994) Seismic sequence in carbonate rocks by vibration liquefication. *Acta Geological Sinica* (English Edition) **7**, 243–265.

Rodríguez-Pascua MA, Calvo JP, De Vicente G and GómezGras D (2000) Soft-sediment deformation structures interpreted as seismites in lacustrine sediments of the Prebetic zone, SE Spain, and their potential use as indicators of earthquake magnitudes during the late Miocene. *Sedimentary Geology* **135**, 117–135.

Salomon ML, Grasemann B, Plan L, Gier S and Schöpfer MPJ (2018) Seismically-triggered soft-sediment deformation structures close to a major strike-slip fault system in the eastern Alps (Hirlatz cave, Austria). *Journal of Structural Geology* **110**, 102–115.

Sarkar S, Banerjee S and Chakraborty S (1995) Synsedimentary seismic signature in Mesoproterozoic Koldaha Shale, Kheinjua Formation, central India. *Indian Journal of Earth Science* **22**, 158–164.

Sarkar S, Choudhuri A, Banerjee S, van Loon AJ and Bose PK (2014) Seismic and non-seismic soft-sediment deformation structures in the Proterozoic Bhander Limestone, central India. *Geologos* **20**, 89–103.

Schnyder J, Baudin F and Deconinck JF (2005) A possible tsunami deposit around the Jurassic-Cretaceous boundary in the Boulonnais area (northern France). *Sedimentary Geology* **177**, 209–227.

Seilacher A (1969) Fault-graded beds interpreted as Seismites. *Sedimentology* **13**, 155–159.

Seth A, Sarkar S and Bose PK (1990) Synsedimentary seismic activity in an immature passive margin basin, lower member of Katrol Formation, Upper Jurassic, Kutch, India. *Sedimentary Geology* **68**, 279–291.

Shanmugam G (2016) The seismite problem. *Journal of Palaeogeography* **5**, 318–362.

Shanmugam G (2021) The turbidite-contourite-tidalite-baroclinite-hybridite problem: orthodoxy vs. empirical evidence behind the Bouma Sequence. *Journal of Paleogeography* **10**, 1–32.

Silva PG, Cañaveras JC, Sánchez-Moral S, Lario J and Sanz E (1997) 3D soft-sediment deformation structures: evidence of quaternary seismicity in the Madrid Basin, Spain. *Terra Nova* **9**, 208–212.

Sims JD (1973) Earthquake-induced Structures in Sediments of Van Norman Lake, San Fernando, California. *Science* **182**, 161–163.

Sims JD (1975) Determining earthquake recurrence intervals from deformational structures in young lacustrine sediments. *Tectonophysics* **29**, 141–152.

Singh A, Deori N, Pandey DK, Shekhawat RS and Verma P (2021) Biostratigraphic Implications of the Calcareous Nannofossils from the Spiti Formation at Langza, Spiti Valle. In *Mesozoic Stratigraphy of India A Multi-Proxy Approach* (eds S. Banerjee and S. Sarkar), pp 429–442. Cham: Springer.

Sun YD, Richoz S, Krystyn L, Grasby SE, Chen YL, Banerjee D and Joachimski MM (2021) Integrated bio-chemostratigraphy of Lower and Middle Triassic marine successions at Spiti in the Indian Himalaya: Implications for the Early Triassic nutrient crisis. *Global and Planetary change* **196**, 1–25.

Takashimizu Y and Masuda F (2000) Depositional facies and sedimentary successions of earthquake-induced tsunami deposits in Upper Pleistocene incised valley fills, Central Japan. *Sedimentary Geology* **135**, 231–239.

Tessier B and Terwindt J (1994) An example of soft-sediment deformations in an intertidal environment - the effect of a tidal bore. *Comptes-Rendus de l'Académie des Sciences Série* **II**, 217–233.

Tian HS, Zhang SH and Zhang AS (2016b) Test investigation on liquefied deformation structure in saturatedlime–mud composites triggered by strong earthquakes. *Acta Geologica Sinica* (English Edition) **90**, 2008–2021.

Van Loon AJ (2009) Soft-sediment deformation structures in siliciclastic sediments: an overview. *Geologos* **15**, 3–55.

Van Loon AJ (2014a) The life cycle of seismite research. *Geologos* **20**, 61–66.

Van Loon AJ, Han Z and Han Y (2013) Origin of the vertically orientated clasts in brecciated shallow-marine limestones of the Chaomidian Formation (Furongian, Shandong Province, China). *Sedimentology* **60**, 1059–1070.

Van Loon AJ and Pisarska-Jamroży M (2014) Sedimentological evidence of Pleistocene earthquakes in NW Poland induced by glacio-isostatic rebound. *Sedimentary Geology* **300**, 1–10.

Vanneste K, Meghraoui M and Camelbeeck T (1999) Late quaternary earthquake-related soft-sediment deformation along the Belgian portion of the Feldbiss fault, lower Rhine graben system. *Tectonophysics* **309**, 57–79.

Wheeler RL (2002) Distinguishing seismic from nonseismic soft-sediment structures: criteria from seismic-hazard analysis. In *Ancient seismites: Geological Society of America Special Paper* (eds F.R. Ettensohn, N. Rast and C.E. Brett), **359**, pp. 1–11.

Yu W, Liang Q, Tian J, Han Y, Wang F and Zhao M (2022) Sedimentary Responses of Late Triassic Soft-Sedimentary Deformation to Paleoearthquake Events in the Southwestern North China Plate. *Minerals* **12**, 1–16.

Zhong N (2017) *Paleoseismic and Provenance Analysis of Late Pleistocene Lacustrine Deposits in Upper Minjiang River*. Institute of Geology, China Earthquake Administrator: Beijing, China.

Zhong N, Jiang H, Li H, Su D, Xu H, Liang L and Fan J (2022) The potential of using soft-sediment deformation structures for quantitatively reconstructing paleo-seismic shaking intensity: progress and prospect. *Environmental Earth Sciences* **81**, 1–22.

Zhong N, Jiang HC, Li HB, Xu HY, Shi W, Zhang SQ and Wei XT (2019) Last deglacial soft-sediment deformation at Shawan on the eastern Tibetan plateau and implications for deformation processes and seismic magnitudes. *Acta Geological Sinica* **93**, 430–450.